A Reliability-Based Method to Quantify the Capacity Value of Soft Open Points in Distribution Networks

Ilias Sarantakos, Natalia-Maria Zografou-Barredo, Da Huo, David Greenwood, *Member, IEEE*

***Abstract*—Soft open points (SOPs) are power electronic devices which provide interconnection between two feeders in place of normally open points in electricity distribution networks. SOPs can continuously control active power flow between feeders and inject reactive power controllably at both nodes, which can be used to provide substantial capacity support to the system. This paper provides a reliability-based method to quantify the capacity value (the additional load which can be accommodated without reducing reliability) of SOPs using the Effective Load Carrying Capability method within a Monte Carlo Simulation (MCS). Optimization of post-fault active/reactive power injections by SOPs to minimize energy not supplied is formulated (directly in matrix form) as a second-order cone programming problem. This results in very low computational times which enables embedding of the optimization problem within the MCS. The proposed methodology is applied to a modified real-world distribution network considering three different SOP sizes (5 SOPs totalling 2.5, 5, 10 MVA) across three redundancy levels (N-1, N-0.75, N-0.5), and on an unbalanced network with distributed generation. Results demonstrate capacity values ranging from 2.4–12.84 MVA. When operating under a relaxed redundancy level, the capacity value of a given SOP capacity can more than double relative to N-1.**

***Index Terms*—Capacity value, distribution network, effective load carrying capability, reliability, soft open point.**

NOMENCLATURE

A. Sets

$k{:}0{\rightarrow}k$	Set of nodes connected to node 0 (substation node).
$k{:}j{\rightarrow}k$	Set of nodes connected to node j except node i.
Ω_b, Ω_n	Set of network branches / nodes.
Ω_{SOP}	Set of nodes with soft open points (SOPs).

B. Indices

i, j	Indices of nodes ($i, j \in \Omega_n$).
l (or ij)	Index of branches (l, $ij \in \Omega_b$).
t	Index of time.

C. Monte Carlo Simulation Variables

C	Available incoming circuit capacity.
D_t	Sampled demand value at simulated hour t.
$EENS$	Expected Energy Not Supplied (EENS).
$EENS_{0C,1C,2C}$	EENS corresponding to 0, 1, 2 circuits being available.
$EENS_t$	EENS at simulated hour t.
ENS_t	Energy Not Supplied at simulated hour t.
k_1, k_2, k_3	Random numbers between 0 and 1.
P_t	Total active demand of the substation under study at t.
R	Rating of one circuit.
S_t^{SOP}	SOP capacity at t (0, if unavailable; S^{SOP}, if available).

D. Monte Carlo Simulation Parameters

A_C	Availability of one incoming circuit.
A_{OHL}, A_{TX}	Availability of the overhead line / transformer.
A_{SOP}	Availability of the SOP.
$p_{0C,1C,2C}$	Probability of 0, 1, 2 circuits being available.
S^{SOP}	SOP capacity.

E. Optimization Variables

a	Proportion of substation demand that can be supplied.
I_{ij}, $I_{ij,max}$	Current magnitude / rating of branch ij (or l).
L_{ij} (or L_l)	Squared current of branch ij (or l).
P_{ij}, Q_{ij}	Active / Reactive power flow from node i to node j.
P_i^G, Q_i^G	Active / Reactive power generation at node i.
$P_{S/S1}$, $Q_{S/S1}$	Active / Reactive power flow through substation S/S 1.
P_i^{SOP}, Q_i^{SOP}	Active / Reactive power injection by SOP at node i.
$P_i^{SOP,L}$	Active power loss of SOP at node i.
V_i, u_i	Voltage magnitude / Squared voltage at node i.

F. Optimization Parameters

LC_i^{SOP}	Loss coefficient of SOP at node i.
P_i^D, Q_i^D	Active / Reactive power demand at node i.
R_{ij}, X_{ij}	Resistance / Reactance of branch ij (or l).
$S_{S/S1}$, S^{SOP}	Capacity of substation under study / SOP capacity.
V_{max}, V_{min}	Maximum and minimum voltage limit.
φ_1, φ_2	Parameters used in the objective function.

G. Reliability Parameters

P_{stuck}	Probability of circuit breaker (CB) failure on demand.
$t_{S/S}$	Substation switching time.
λ, r, U	Failure rate / Repair time / Unavailability.

H. Failure Modes

A	Active failure (and successful operation of CBs).
A+S	Active failure in combination with a stuck CB.
P	Passive failure.

I. INTRODUCTION

SOFT OPEN POINTS (SOPs) are power electronic devices which interconnect two feeders in place of conventional switches in electricity distribution networks (DNs) [1]. Two characteristics of SOPs, which can provide substantial benefits to the operation and planning of modern DNs, are: 1) the ability to provide continuous active power flow regulation between the interconnected feeders; and 2) the capability to inject reactive power independently at both AC terminal nodes [2].

A key problem in DN planning is to minimize capital investment to meet the growing and changing demand in a reliable way [3]. SOPs can enhance the loadability of existing networks, thereby defering or avoiding network reinforcement [2]. This paper proposes a reliability-based framework to quantify the capacity value (the additional load that can be accommodated when they are added to the network) of SOPs.

A. Literature Review

This section addresses capacity value and soft open points.

1) Capacity Value

According to the effective load carrying capability (ELCC) methodology [4] – which is widely used [5-7] and generally regarded as a benchmark for capacity value assessment [8, 9]. The capacity value of an asset is the additional load that can be accommodated without reducing system reliability. Quantifying the capacity value of assets can support network investment decisions, which may be required when network constraints exist (either during normal or fault conditions).

ELCC requires: 1) a reliability index; and 2) a reliability evaluation methodology. Hegazy *et al.* [10] present a general method to evaluate the ability of a DN to satisfy its demand in presence of distributed generation (DG). A two-state model is employed to simulate the operation of each DG and a Monte Carlo Simulation (MCS) is used to evaluate the average unsupplied load per hour. Konstantelos *et al.* [11] assesses the capacity value of energy storage using sequential MCS and expected energy not supplied (EENS). Sequential simulation is required to capture the impact of time-dependent variables, such as state of charge. In [7], the authors quantify the capacity value of network reconfiguration (NR) using sequential MCS integrated, using mixed-integer second-order cone programming (SOCP) for the optimal NR problem. However, to achieve this integration, which is extremely computationally intensive, they use a relaxed optimality gap, which does not solve the optimization problem to optimality. References [7, 11] use multiple redundancy levels (explained in Section III-B) to expose its impact on the capacity value. Networks with relaxed redundancy levels (e.g. N-0.75 and N-0.5) are gaining attention from researchers and DN operators because they can unlock capacity without compormising reliability [7, 11, 12].

To quantify capacity value, this paper employs: 1) The ELCC capacity value assessment methodology. 2) MCS for reliability evaluation. 3) The EENS reliability index, which accounts for the frequency, duration, and severity of failures. EENS has also been used in [7, 11, 13] and is the customary index in similar studies in Great Britain [8]. EENS considers both the probability and consequence (energy not supplied) of a failure, in contrast to Loss of Load Expectation (LOLE), which only a measure of probability, neglecting consequence [14]. 4) Three redundancy levels (N-1, N-0.75, and N-0.5).

2) Soft Open Points

From an SOP planning perspective, Giannelos *et al.* [15] propose a stochastic model which considers investment in SOPs and conventional assets to tackle network constraints. Konstantelos *et al.* [16] propose a stochastic planning model which also considers demand side response and coordinated voltage control. Both [15] and [16] employ stochastic mixed-integer nonlinear programming. In [17], a coordinated planning model for DG and SOPs is presented; it is formulated as a bi-level optimization problem which is then reformulated into a single-level mixed-integer SOCP problem. Existing planning models optimize the investment and operational cost of the system without quantifying the capacity value of SOPs. Evaluating the capacity value of SOPs is significant because it allows comparison with conventional network reinforcement measures and other Smart Grid alternatives.

Limited research sought to quanitify the additional demand that can be accommodated by SOPs. The authors of [2] maximize the load growth factor that applies to a single loading condition of the network without violating any thermal or voltage constraints; they employ a deterministic approach which neglects the uncertainty and variability of demand. To appropriately handle these characteristics, this paper proposes a probabilistic, reliability-based model which considers a wide range of loading conditions and the reliability of substations, incoming circuits, and SOPs. In [2], the demand is assumed to be either fully supplied or not; this paper accounts for states in which the demand can be partially served, and employed a reliability metric that considers the energy not supplied during each failure. This flexible approach allows different levels of reliability to be considered by the decision maker.

B. Contribution and Organization of the Paper

The paper advances the state of the art in the following ways:

1) The development of a novel, reliability-based method to quantify the capacity value of soft open points in the presence of time variant load, and accounting for the reliability of the existing infrastructure and SOPs.
2) An accurate and efficient optimization method which enables the globally optimal operation of SOPs – with an objective of minimizing energy not supplied (ENS) – to be embedded within the MCS by solving each optimization problem in tens of milliseconds.
3) The impact of existing network design on SOP capacity value is investigated by considering three redundancy levels (N-1, N-0.75, N-0.5).
4) The impact of protection systems (specifically circuit breakers) and their different failure modes, is represented in the model and its effect on ELCC is quantified.

II. METHODOLOGY

This section presents a methodology which evaluates the reliability of an existing network, optimizes the actions of SOPs installed in that network to improve reliability, and computes the capacity value as the additional demand that can be accommodated whilst maintaining the reliability of the original system. This is divided into: A) assumptions and clarifications; B) the ELCC capacity value methodology; C) the MCS framework; and D) the SOP optimization to minimize ENS.

A. Assumptions

1) This study focuses on the security of supply of the primary substation as in [7, 11, 13]. The considered redundancy levels (N-1, N-0.75, and N-0.5) refer to the associated incoming circuits (33 kV lines and transformers). Only faults in the incoming circuits are considered.
2) SOPs are immediately (optimally) rescheduled following a fault in the incoming circuits.

B. ELCC-Based Capacity Value

The concept of the ELCC-based capacity value was introduced in Section I-A1, and is illustrated in Fig. 1. ELCC is defined as the additional load (ΔD) that can be supplied using a network intervention, in this case SOPs, while maintaining the same EENS as the base case. The definition of EENS is:

$$EENS = \sum p_x \cdot ENS_x \tag{1}$$

where p_x is the probability of the system being in a given operational state, x; and ENS_x is the ENS in that state [13]. In any real system with varying demand, the number of states is intractably large, so a stochastic method – in this case MCS – is required to fully explore the state space.

The capacity value of SOPs is calculated as follows (Fig. 1):

1) The base case EENS is evaluated (initial load, no SOPs).
2) SOPs are added to the system; this will reduce the EENS, so the EENS is re-evaluated.
3) The load is then incrementally increased, which causes the EENS to rise, until the EENS reaches the base case value.
4) The load growth (ΔD) for which the EENS with the SOPs equals that of the base case is the SOP capacity value.

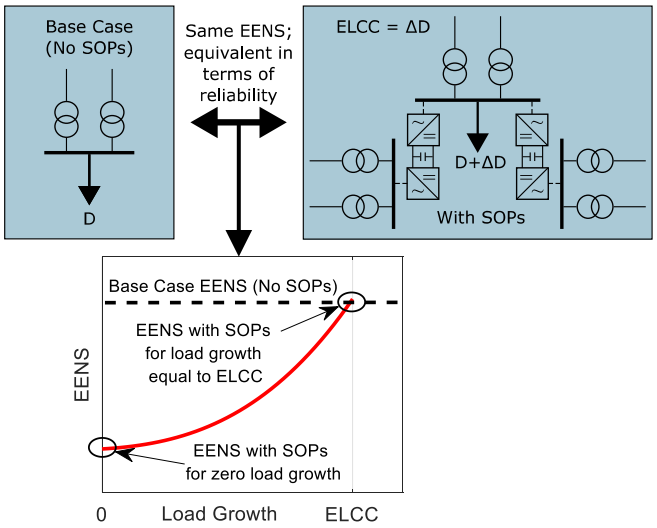

Fig. 1. The main concept of the ELCC methodology for soft open points.

C. EENS Evaluation via Monte Carlo Simulation

MCS stochastically explores the state space shown in (1) by simulating thousands of years of system operation. Fig. 2 provides an overview of the MCS algorithm. Separate simulations are performed for each value of incoming capacity C (corresponding to two, one, or zero circuits available) in each season. The availability (A) of a network component can be calculated using [14]:

$$A = (\text{up time})/(\text{total time}) = (8760 - \lambda r)/8760 \quad (2)$$

where total time = up time + down time; λr expresses the down time of a component in h/y; therefore, up time is $8760 - \lambda r$. Assuming the substation is supplied by two circuits (as in Fig. 1), and each circuit comprises an overhead line (OHL) and a transformer (TX), the availability of each circuit (A_C) is:

$$A_C = A_{OHL} \cdot A_{TX} \quad (3)$$

At each timestep (t) demand (D_t) is sampled with replacement from the historical demand data, and the SOP availability is calculated. If demand is lower than the available incoming circuit capacity ($D_t < C$), then there is sufficient capacity to supply all customers and $ENS_t = 0$. If the demand is greater than the incoming circuit capacity ($D_t > C$), the network is not adequate and the SOPs must help to supply demand. SOP operation is optimized (see Section II-D) to minimize the ENS. In this case, $ENS_t = (1 - a) \cdot P_t$, where P_t is the total active demand of the substation, and a is the proportion of demand served. $EENS_t$ is then evaluated and the simulation continues until one of the stopping criteria are met.

The simulation depicted in Fig. 2 is carried out separately for each network state; this state space partitioning [13] enables the impact of incoming circuit availability to be studied without the need to rerun the MCS; it also avoids running thousands of unnecessary simulations in states which do not require any action from the SOPs. The probability the available incoming circuit capacity (C) is in a given state is calculated as follows:

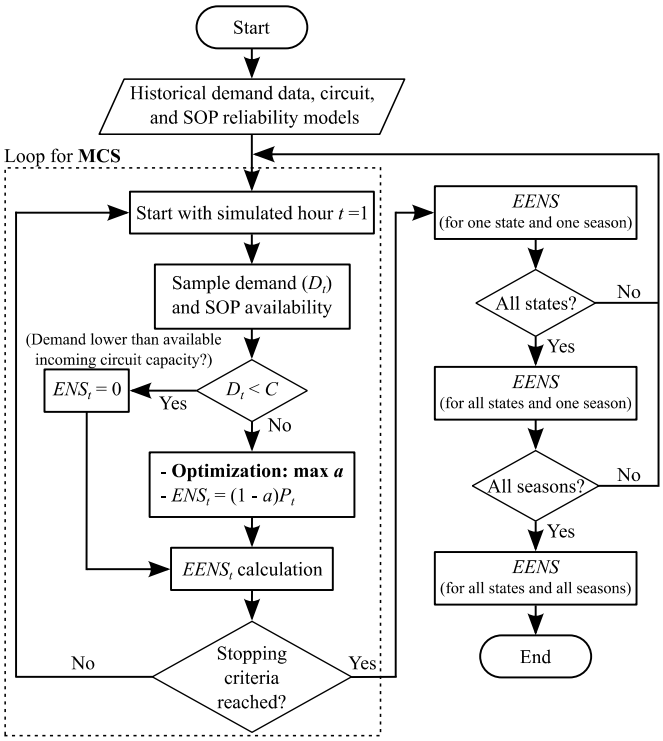

Fig. 2. Overview of the MCS algorithm used to evaluate system reliability.

$$p_{0C} = (1 - A_C)^2,\ p_{1C} = 2(1 - A_C) - p_{0C},\ p_{2C} = 1 - p_{1C} - p_{0C} \quad (4)$$

These yield capacities of 0, R, and $2R$, where R is the single circuit rating (the lower of the OHL and transformer rating).

$$\begin{aligned} C = 2R &\Rightarrow EENS_{2C} = 0 \\ C = R &\Rightarrow EENS_{1C} = EENS_{MCS} \\ C = 0 &\Rightarrow EENS_{0C} = EENS_{MCS} \end{aligned} \quad (5)$$

Because the maximum demand remains below the double circuit capacity in all but the most extreme cases, $EENS_{2C}$ is zero and requires no simulation. $EENS_{1C}$ and $EENS_{0C}$, however, do require simulation and are calculated as described below.

In each iteration of the MCS, demand (D_t) is sampled from the historical data and SOP availability is derived as follows:

$$\begin{aligned} k_3 < A_{SOP} &\Rightarrow \text{SOP available} \Rightarrow S_t^{SOP} = S^{SOP} \\ k_3 > A_{SOP} &\Rightarrow \text{SOP unavailable} \Rightarrow S_t^{SOP} = 0 \end{aligned} \quad (6)$$

When an SOP is unavailable, its capacity is set to zero; otherwise, SOP rated capacity is used. ENS_t – depending on D_t and C – is derived as:

$$ENS_t = \begin{cases} 0, & D_t < C \\ (1 - a) \cdot P_t, & D_t > C \end{cases} \quad (7)$$

where a is the output of the optimization problem formulated in Section II-D, and expresses the proportion of the substation

demand that can be supplied via the available incoming circuit capacity and SOP contribution. Subsequently, using *ENS* from simulated hour 1 to *t*, the $EENS_t$ (per calendar year) is given by:

$$EENS_t = \left(8760/t\right) \cdot \sum_{t'=1}^{t} ENS_{t'} \tag{8}$$

Equation (8) assumes that each hour of the historical demand data has an equal probability of occurrence. Convergence is determined using the Coefficient of Variation (CoV) of the EENS at simulated hour *t* ($\text{CoV}_{EENS,t}$):

$$CoV_{EENS_t} = \text{std}\left(EENS(1:t)\right) \big/ \text{mean}\left(EENS(1:t)\right) \tag{9}$$

The CoV of the EENS is computed every 100 simulated hours to reduce the number of calculations; when CoV drops below 5% [18], the MCS terminates. A second stopping criterion is also used for EENS values very close to zero, as the first criterion is not suitable in this case [11]. The second criterion checks the change of the EENS over the last 10,000 simulated hours, and terminates the algorithm if it is less than 1%. Then, the EENS for all incoming circuit states is:

$$EENS_{\text{all states}} = p_{0\text{C}} EENS_{0\text{C}} + p_{1\text{C}} EENS_{1\text{C}} + p_{2\text{C}} \underbrace{EENS_{2\text{C}}}_{0} \tag{10}$$

The EENS is evaluated for each season separately due to seasonal variations in demand and OHL ratings; the final EENS is the weighted sum of results for each season [19].

$$EENS_{\text{final}} = \frac{3}{12} EENS_{\text{win}} + \frac{2}{12} EENS_{\text{spr}} + \frac{4}{12} EENS_{\text{sum}} + \frac{3}{12} EENS_{\text{aut}} \tag{11}$$

D. Optimization of SOP Operation

The post-fault operation of the SOPs will have a substantial impact on their capacity value; fast, accurate models which can determine the optimal power injections are a critical component of the proposed methodology. This section describes the optimization carried out to minimize the unsupplied demand when the available incoming circuit capacity is not adequate. The objective is to optimize the active and reactive power injections of the SOPs to maximize the proportion of demand (*a*) that can be supplied, thereby minimizing ENS_t. The original problem is a nonconvex, nonlinear optimization problem; global optimality cannot be guaranteed, and solution methods are too computationally demanding to be embedded in an MCS. To formulate the SOP optimization as a convex problem, two relaxations have been made: the first corresponds to power flow equations (equation (17)) [20, 21], and the second corresponds to SOP losses (equation (27)) [22]. In the following subsections, the optimization problem components are presented: 1) the constraints; 2) the objective function; and 3) the whole model.

1) Constraints

This section presents the constraints of the optimization problem (power flow equations and SOP constraints) and their corresponding relaxations. Power flow equations are based on *DistFlow branch equations* [23, 24] considering the convex relaxation in [20, 21]; SOP constraints are implemented according to [22].

a) Power Flow Equations

The *DistFlow branch equations* [20] are presented below for each branch *l* (*ij*) $\in \Omega_\text{b}$. These equations use the active and reactive power flows, as well as the voltage magnitude (voltage angle is not used) at one end of the branch to express the same quantities at the other end of the branch [23, 24]. Fig. 3 provides a graphical representation. The definition of variables u_i and L_{ij} facilitates the convex formulation of the power flow model.

$$P_{ij} = \sum_{k:j\to k} P_{jk} + R_{ij} L_{ij} + P_j^{\text{D}} - P_j^{\text{G}}, \ \forall\ ij \in \Omega_\text{b} \tag{12}$$

$$Q_{ij} = \sum_{k:j\to k} Q_{jk} + X_{ij} L_{ij} + Q_j^{\text{D}} - Q_j^{\text{G}}, \ \forall\ ij \in \Omega_\text{b} \tag{13}$$

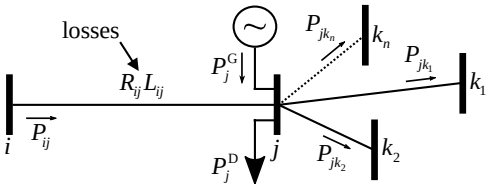

Fig. 3. Graphical representation of the *DistFlow branch equations*. The (active / reactive) power flow at the sending node of branch *ij* is equal to the sum of: i) sum of power flows from node *j* to nodes k_1, k_2,…, k_n, ii) branch losses, iii) demand at node *j*, and iv) minus generation at node *j*.

$$u_j = u_i - 2\left(R_{ij} P_{ij} + X_{ij} Q_{ij}\right) + \left(R_{ij}^2 + X_{ij}^2\right) L_{ij}, \ \forall\ ij \in \Omega_\text{b} \tag{14}$$

where

$$u_i = V_i^2, \ \forall\ i \in \Omega_\text{n} \tag{15}$$

$$L_{ij} = \left(P_{ij}^2 + Q_{ij}^2\right) \big/ u_i = I_{ij}^2, \ \forall\ ij \in \Omega_\text{b} \tag{16}$$

which is relaxed to [20, 21]:

$$\left\| 2P_{ij} \quad 2Q_{ij} \quad L_{ij} - u_i \right\|_2 \le L_{ij} + u_i \tag{17}$$

Incorporating SOP active and reactive power injections, as well as *a*, (12) and (13) become:

$$P_{ij} - \sum_{k:j\to k} P_{jk} - R_{ij} L_{ij} = \underbrace{a \cdot P_j^{\text{D}}}_{\text{S/S 1}} \ (\text{or} \ \underbrace{P_j^{\text{D}}}_{\text{S/S 2}}) - \underbrace{P_j^{\text{SOP}}}_{\text{if SOP at node } j} \tag{18}$$

$$Q_{ij} - \sum_{k:j\to k} Q_{jk} - X_{ij} L_{ij} = \underbrace{a \cdot Q_j^{D}}_{\text{S/S 1}} \ (\text{or} \ \underbrace{Q_j^{D}}_{\text{S/S 2}}) - \underbrace{Q_j^{\text{SOP}}}_{\text{if SOP at node } j} \tag{19}$$

where S/S 1 is the substation under study, i.e. the substation to which SOPs provide capacity support. S/S 2 is the substation that assists S/S 1, i.e. takes up additional load to relieve S/S 1 when demand of S/S 1 (D_t) cannot be supplied by the available incoming circuit capacity (*C*). In (18) and (19), factor *a* applies to demand of load points of substation S/S 1 only, because we are interested in the maximum demand that can be supplied through the available incoming circuit capacity and SOPs for the substation under study (S/S 1). At the nodes at which an SOP is connected the associated active and reactive power injections are included in (18) and (19), respectively.

The proportion of substation demand that can be supplied (*a*) ranges between zero and one, with zero meaning that no substation demand can be supplied, and one indicating that the full substation demand can be met. This is expressed as follows:

$$0 \le a \le 1 \tag{20}$$

Network operational constraints are described below:

$$V_{\min}^2 \le u_i \le V_{\max}^2, \ \forall\ i \in \Omega_\text{n} \tag{21}$$

$$L_{ij} \le I_{ij,\max}^2, \ \forall\ ij \in \Omega_\text{b} \tag{22}$$

$$\left\| P_{\text{S/S1}} \quad Q_{\text{S/S1}} \right\|_2 \le S_{\text{S/S1}} = C, \ P_{\text{S/S1}} = \sum_{k:0\to k} P_{0k}, \ Q_{\text{S/S1}} = \sum_{k:0\to k} Q_{0k} \tag{23}$$

Equation (23) represents the capacity limit of substation S/S 1. Note that the right-hand side of this constraint is variable

(function of C), depending on the number of available circuits. $P_{S/S1}$ and $Q_{S/S1}$ are the sums of active and reactive power flows of all outgoing feeders from the low voltage busbar of S/S 1.

b) SOP Constraints

This section presents the model of an SOP connecting nodes i and j [22]:

$$P_i^{SOP} + P_j^{SOP} + P_i^{SOP,L} + P_j^{SOP,L} = 0 \quad (24)$$

$$P_i^{SOP,L} = LC_i^{SOP}\sqrt{\left(P_i^{SOP}\right)^2 + \left(Q_i^{SOP}\right)^2}, \text{ nodes } i, j \quad (25)$$

$$\left\| P_i^{SOP} \quad Q_i^{SOP} \right\|_2 \le S_i^{SOP}, \text{ nodes } i, j \quad (26)$$

Equation (24) expresses the active power balance of an SOP including SOP power losses at nodes i and j which are defined in (25), respectively. There are two separate loss terms for each side, as there is a converter associated with each node. Equation (26) represents the SOP capacity constraints; depending on SOP availability (equation (6)), the corresponding capacity can be either S^{SOP} or zero. Constraint (25) is relaxed to:

$$\left\| P_i^{SOP} \quad Q_i^{SOP} \right\|_2 \le P_i^{SOP,L} \Big/ LC_i^{SOP} \quad (27)$$

2) Objective Function

The objective (28) is to maximize the proportion of the substation demand (a) that can be supplied. There are two additional terms in the objective function whose inclusion ensures exactness of the relaxations made in this model (i.e. that the relaxed inequalities are tight in the optimal solution). The second term ensures the gaps of the first set of relaxed constraints (related to power flow equations – (17)) are small; likewise, the third term reduces the gaps from the second relaxation (for SOP losses – (27)). Decreasing the values of L_{ij} results towards making the relaxed constraints in (17) active at optimality [21]. Likewise, decreasing $P_i^{SOP,L}$, leads towards making active the relaxed constraints in (27). Such an approach has also been employed in [25].

$$\text{maximize } a - \phi_1 \cdot \sum_{ij \in \Omega_b} L_{ij} - \phi_2 \cdot \sum_{i \in \Omega_{SOP}} P_i^{SOP,L} \quad (28)$$

where φ_1 and φ_2 are two weights with appropriate values, whose determination is provided in Appendix A.

3) Model

The decision variables of the optimization problem are: u_i, P_{ij}, Q_{ij}, L_{ij}, a, P_i^{SOP}, Q_i^{SOP}, $P_i^{SOP,L}$, $P_{S/S1}$, and $Q_{S/S1}$. The SOCP model solved within the MCS (see Fig. 2) when $D_t > C$, is:

maximize (28), subject to (14), (17)-(24), and (26)-(27)

III. Case Study

A. Test Network

The test network is based on a real DN operated by Taiwan Power Company (TPC) [26] and has been modified as follows: 1) normally open branches 86, 89, 90, 92, 93, 94, 95, and 96 have been removed; and 2) normally open branches 84, 85, 87, 88, and 91 have been replaced with SOPs. The modified TPC DN is shown in Fig. 4. It is an 11.4 kV network with 11 feeders and 5 SOPs. The customer types for each load point are taken from [27]. This network (which is widely used in the relevant literature [7, 17]) was selected because it has two substations, which allows load transfer from S/S 1 through SOPs to S/S 2 when the available incoming circuit capacity is insufficient to supply S/S 1 demand. The upstream network circuits (overhead lines and transformers) that supply the modified TPC DN are presented in Fig. 5. UK medium voltage distribution limits (0.94 – 1.06 pu) [28] are used; substation voltage is set at 1.06 pu. Feeder seasonal ratings are shown in Table I [29].

B. Electricity Demand Data

The electricity demand data have been taken from [7], and correspond to three redundancy levels: N-1, N-0.75, and N-0.5 [11]. N-k means that all demand must be supplied with any k circuits on outage [8]. More than one redundancy level is used to demonstrate its impact on the capacity value. The redundancy level determines the maximum peak demand:

1) N-1: Peak demand must be met in the case of a single circuit outage (a peak demand of 16 MVA).
2) N-0.75: Peak demand must be supplied in the case of an "outage" of 0.75 circuits (a peak demand of 20 MVA).
3) N-0.5: Peak demand must be met in the case of an "outage" of 0.5 circuits (a peak demand of 24 MVA).

The hourly cumulative loading probabilities at substation S/S 1 during winter for each redundancy level are shown in Fig. 6.

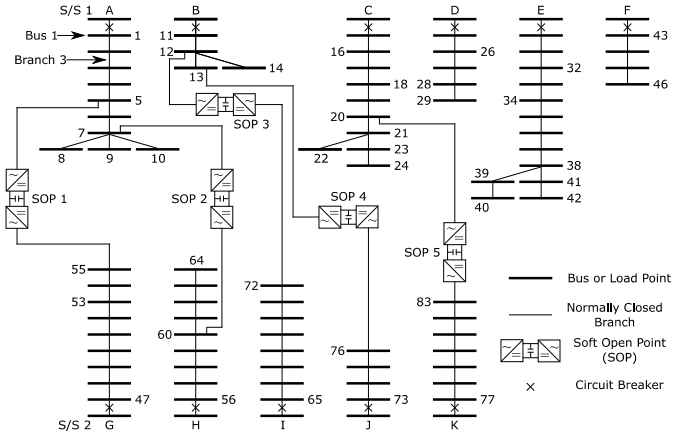

Fig. 4. The modified TPC DN. Substation S/S 1 supplies feeders A–F; substation S/S 2 supplies feeders G–K.

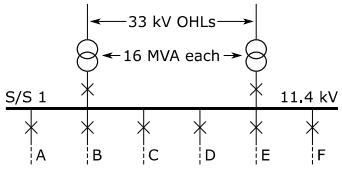

Fig. 5. The upstream network circuits that supply S/S 1 of the TPC DN.

TABLE I
11 kV Feeder Thermal Limits

Season	Winter	Spring/Autumn	Summer
Limit (MVA)	12.55	11.79	10.65

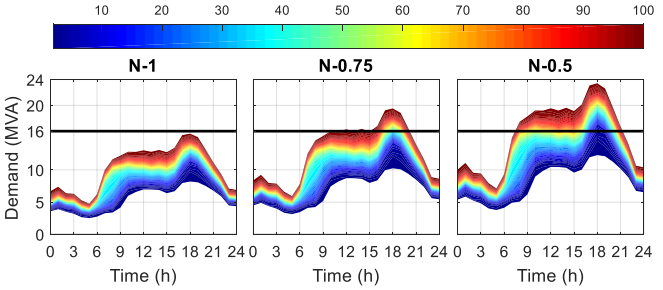

Fig. 6. Substation S/S 1 loading level for each redundancy level (winter). The colour bar indicates the cumulative probability of each loading level. The black line represents the capacity of a single transformer.

C. Reliability Data

Each incoming circuit of substation S/S 1 comprises an 11 km 33 kV overhead line and a transformer. The reliability data for these assets are presented in Table II [30]. The overall availability for each circuit is 99.951% (unavailability 4 h/y).

TABLE II
RELIABILITY DATA

Asset	Failure Rate (λ)	Repair Time
Transformer	0.015 f/y	15 h
33 kV OHL	0.046 f/y·km	8 h

IV. RESULTS

The proposed methodology was applied to the modified TPC DN using the data presented in Section III. The MCS and the optimization model were implemented using MATLAB R2017a; optimization was performed using Gurobi [31]. An Intel Core i7 quad-core processor at 1.9 GHz with 16 GB of RAM was used for the simulations.

The base case corresponds to 1) no SOPs; and 2) zero load growth. Three SOP ratings were considered: 0.5 MVA, 1 MVA, and 2 MVA. SOP availability is assumed to be 99.91%, which corresponds to a down time of 8 h/y. Loss coefficients for SOPs are assumed to be 0.02 [22]. The following subsections present: A) the ELCC results for three SOP sizes and three redundancy levels; B) the computational performance of the proposed model; C) a comparison with the full nonconvex AC Optimal Power Flow (ACOPF) model; D) a comparison with the capacity value provided by network reconfiguration [7]; E) the impact of CB failures on the capacity value of SOPs; and F) the impact of DG and modified X/R ratios in an unbalanced DN.

A. ELCC Results

This section presents the results for the ELCC-based capacity value for 5 SOPs in the modified TPC DN at three redundancy levels and three SOP capacities. The base case (no SOPs, zero load growth) yields EENS results of 4.21 MWh/year, 0.49 MWh/year, and 0.017 MWh/year for the N-0.5, N-0.75, and N-1 redundancy levels, respectively. When SOPs are added to the network, the EENS falls. The demand was then increased incrementally, causing the EENS to rise; the load growth for which the EENS reached constituted the ELCC. The results are shown in Fig. 7, which illustrates the ELCC in MVA and as a percentage of the total SOP capacity installed in the network.

From these results, we can make the following observations:

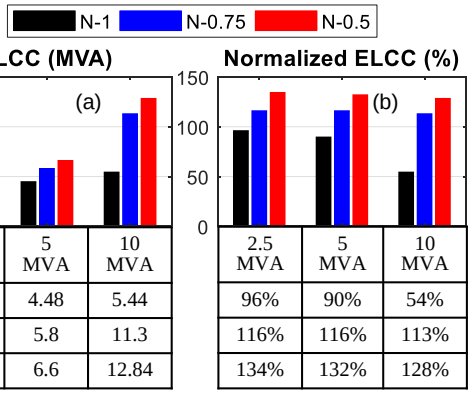

	2.5 MVA	5 MVA	10 MVA	2.5 MVA	5 MVA	10 MVA
N-1	2.4	4.48	5.44	96%	90%	54%
N-0.75	2.9	5.8	11.3	116%	116%	113%
N-0.5	3.36	6.6	12.84	134%	132%	128%

Fig. 7. ELCC in MVA (a), and normalized ELCC (b) (percentage of total SOP capacity) versus total SOP capacity (2.5 MVA, 5 MVA, and 10 MVA) for three redundancy levels (N-1, N-0.75, and N-0.5).

1) When operating under a relaxed redundancy level, significantly more additional demand can be accommodated (from +40% for a total SOP capacity of 2.5 MVA to +136% for a total SOP capacity of 10 MVA). The lower the initial reliability level of the network (or the higher the acceptable EENS), the higher the capacity contribution of the SOPs.
2) Smaller SOP sizes achieve a higher normalized ELCC. This is because SOPs with lower capacity have higher utilization, i.e. they operate at higher power than larger units relative to their rated power. Note that when SOPs are required to support the network during a fault, they do not always operate at maximum power because in a single circuit outage, the power shortfall (difference between demand and single circuit capacity) can be smaller than SOP rated power.
3) For relaxed redundancy levels (N-0.75 and N-0.5), the normalized ELCC is greater than 100%, which means the additional demand that can be accomodayed thanks to the SOPs exceeds the total SOP capacity. This can be justified by the higher acceptable EENS defined by the base case.
4) Under N-1 redundancy level, double circuit outages are the primary driver of EENS. At relaxed redundancy levels, single circuit outages become the main driver, which increases the role of SOPs in ensuring security of supply.

Some additional or alternative approaches could be taken to prioritise customer supplies over system constraints. These could be included in the proposed methodology by altering the asset ratings appropriately. Examples of this include:

1) Cyclic rating of transformers, which would allow increased incoming circuit capacity following a circuit failure; for example, 20.8 MVA (instead of 16 MVA), which corresponds to 130% of the rating of one transformer [32].
2) Real time thermal ratings [33] of lines and transformers, which would allow exploitation of unused headroom due to the cooling effect of the environment; this would increase network capacity during single circuit outages.

B. Computational Performance

For each simulation, the model was optimized (with different input data each time) an average of 77,000 times. The associated computational time was 18 minutes, and the average optimization time was 12ms. This impressively low computational time was achieved via convex (SOCP) optimization and formulation of the problem directly in matrix form without using an optimization modelling language, which would introduce significant additional computational overhead.

To illustrate this, the model was also built and optimized using YALMIP [34], which is a toolbox for modelling and optimization in MATLAB, and it required approximately an extra 0.6s for a single optimization run (see Section IV-C). This time includes the conversion from the user's representation of the problem to matrix form; for the 77,000 optimization runs mentioned above, this additional time corresponds to 12.8h.

C. Comparison with the Full ACOPF Model

This section compares the optimization results using the convex SOCP model proposed in this paper with the full ACOPF model, which is nonconvex and nonlinear. For the latter model, the two extra terms in (28) were not considered, as the full model does not employ any relaxations. The full nonconvex nonlinear programming (NLP) problem is:

maximize a, subject to (14), (16), and (18)-(26)

The full ACOPF model was formulated using YALMIP toolbox [34] in MATLAB R2017a, and was optimized using the fmincon solver. The test case for the comparison was the maximum loading condition (D_t = 24 MVA) with one incoming circuit on outage (C = 16 MVA), and the rating of each SOP was 1 MVA. The comparison of the two models is shown in Table III. The proposed convex SOCP model obtains the same value for a (maximum proportion of S/S 1 demand that can be supplied) within a computational time which is 1,573 times lower than the corresponding time required by the full ACOPF model. Moreover, the relaxed second-order cone constraints are tight at optimality, as shown by the low gap values in Table III, which indicates satisfactory performance of the relaxations. These gaps are defined and evaluated in Appendix A. The results demonstrate the effectiveness and accuracy of the proposed convex SOCP model. A comparison (in terms of computational time) is also made with the solution of the SOCP model using YALMIP. The conversion of the model to matrix form imposes an additional computational overhead of 0.6s.

TABLE III
COMPARISON OF THE PROPOSED CONVEX SOCP MODEL WITH THE FULL (NONCONVEX) ACOPF MODEL

	Convex SOCP		Nonconvex NLP
	Matrix Form	YALMIP	YALMIP
a	0.8900	0.8900	0.8900
Gap_1^* (A)	0.023	0.023	0 (benchmark)
Gap_2^* (MW)	1.49×10^{-6}	1.49×10^{-6}	0 (benchmark)
Comp. Time (s)	0.012	0.612 (0.012 + 0.6)**	18.87 (18.3 + 0.57)**

*See Appendix A.
**Solver time + YALMIP time.

D. Comparison with Network Reconfiguration [7]

This section provides a comparison between the capacity value of SOPs and that of conventional switches with network reconfiguration (NR) capability [7]. The study in [7] used the same case study network as this paper, with a base case in which there was no interconnection, and investigated NR with both manual and remote control switches. Fig. 8 presents the difference between the ELCC of SOPs and the ELCC of manual and remote control NR [7], which correspond to switching times of 1 hour and 15 minutes, respectively.

As shown in Fig. 8, in most cases SOPs provide more capacity value than conventional switching, but in some cases (particularly for small SOPs at lower redundancy levels), the conventional switching could reliably supply more customers. NR – as with SOPs – was able to provide greater capacity support under a relaxed redundancy level (N-0.75 and N-0.5); this is because the less reliable the network is, the more NR and SOPs can contribute (see observation 1 in Section IV-A).

There are three points of note:

1) NR is limited by the branch capacity limits which are no lower than 10.65 MVA (see Table I) in this case study; this allows NR to provide a greater contribution than SOPs, whose capacity never exceeds 2 MVA for each device.
2) Switching time for NR significantly impacts EENS, while SOPs can be rescheduled immediately after a fault.
3) SOPs can provide precise control of the power supplied through each branch, while conventional switching can only adjust the loading in discrete steps.

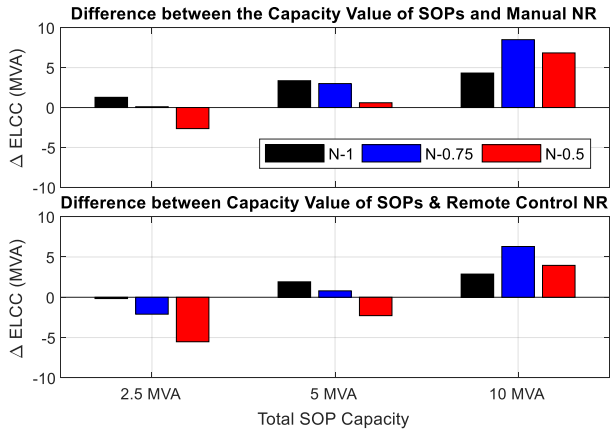

Fig. 8. Difference between the capacity value of SOPs and manual/remote control network reconfiguration. $\Delta\text{ELCC} = \text{ELCC}_{\text{SOP}} - \text{ELCC}_{\text{NR}}$.

The results suggest that SOPs can provide higher capacity support than NR provided they have sufficient power capacity.

E. Impact of Circuit Breaker Failures on ELCC

This section examines how the different failure modes of circuit breakers (CBs) affect the capacity value of SOPs. The following three failure modes are considered in this study [14]:

1) Active failures in the incoming circuits in combination with a stuck CB (the breaker fails to open when required). The corresponding probability (P_{stuck}) is taken from [35].
2) CB active failures.
3) CB passive failures.

An active failure causes the response of the primary protection zone around the failed component (i.e. all nearest CBs operate to clear the fault); examples are short circuits. In contrast, a passive failure does not cause the operation of the breakers; examples are inadvertent opening of CBs and open circuits [14]. P_{stuck} is defined as [14]:

$$P_{\text{stuck}} = \frac{\text{number of times CB fails to open when required}}{\text{number of times CB is requested to open}} \quad (29)$$

The contribution of each failure event to single and double circuit outage probabilities, p_{1C} and p_{0C}, are analyzed and quantified in Appendix B.

Having obtained values for p_{0C}, p_{1C}, and p_{2C} which account for the impact of CBs, we can evaluate the new ELCCs of SOPs for all ratings and redundancy levels. The new base case EENS are 4.61 MWh/year, 0.87 MWh/year, and 0.157 MWh/year for the N-0.5, N-0.75, and N-1 redundancy levels, respectively. p_{1C} increased by 0.5%, whilst p_{0C} rose 920%. The large increase in p_{0C} is becasue CB faults introduce failures which lead to a double circuit outage with a much higher probability than that of two overlapping single circuit outages. Section IV-A states that under N-1 redundancy level, double circuit outages are the main driver of EENS, while at N-0.75 and N-0.5, single circuit outages drive the EENS. Therefore, it is expected that ELCC will change significantly for N-1 but much less for N-0.5.

The changes in ELCC, due to inclusion CB failures, are shown in Table IV. Capacity value increases in all cases. This is in line with observation 1 in Section IV-A, which states that the lower the initial reliability level, the greater the capacity value of SOPs. A lower initial reliability level means (roughly) more failures, which enables the SOPs to contribute more frequently, resulting in a greater ELCC. Consequently, the

inclusion of CB failures leads to increased capacity values, which for this case study are between 0.47% – 11.25%. Finally, as expected, smaller changes are seen for relaxed redundancy levels, with the greatest increases being noticed at N-1.

TABLE IV
INCREASE IN ELCCS DUE TO CIRCUIT BREAKER FAILURES

Red. Level\Total SOP Capacity	Increase in ELCC 2.5 MVA	5 MVA	10 MVA
N-1	+11.25%	+9.38%	+5.88%
N-0.75	+5.52%	+2.59%	+1.24%
N-0.5	+2.38%	+1.06%	+0.47%

F. Unbalanced Distribution Network, DG, and X/R Ratio

This section investigates the impact of DG and lower X/R ratios in an unbalanced DN. For the unbalanced three-phase power flow, a semidefinite programming (SDP) relaxation is employed for the branch flow model (BFM) [36]. The BFM-SDP model has been employed for the power flow equations (equations (10a) – (10f) from [36]), and equations (1), (26)-(28) from [37] have been used for SOPs. The X/R ratio in the TPC DN is approximately 2, across all branches. In this section, each branch reactance (X) is divided by 4, giving X/R ratios below 1. The load on each phase (a, b, c) is set to 39%, 31%, and 30% of the total load, respectively (as in [17]). Finally, eight single-phase photovoltaics (PVs) (generation profiles are from the North-East of England, in 2019, according to [38]) have been considered at the network, as shown in Table V.

TABLE V
PV INSTALLATION PARAMETERS

Parameter	PVs							
Location (Bus)	4	7	12	18	23	28	35	45
Phase	c	b	a	b	a	c	a	b
Capacity (kVA)	250	250	250	250	250	250	250	250

The results of this simulation (using YALMIP [34] and MOSEK [39]) are presented in Table VI. The new base case EENS are 3.63 MWh/year, 0.36 MWh/year, and 0.016 MWh/year for the N-0.5, N-0.75, and N-1 redundancy levels, respectively. A higher base case reliability – primarily because of the installation of PVs, and secondarily due to the lower branch reactances, meaning lower losses – leads to lower ENS when failures occur. Consequently, the SOPs contribute to a lesser extent (i.e. supply less energy) resulting in lower ELCCs (7% – 40%). This agrees with observation 1 in Section IV-A.

TABLE VI
DECREASE IN ELCCS DUE TO PVS AND MODIFIED X/R RATIOS IN AN UNBALANCED DISTRIBUTION NETWORK

Red. Level\Total SOP Capacity	ΔELCC 2.5 MVA	5 MVA	10 MVA
N-1	-7.1%	-10.6%	-14.8%
N-0.75	-18.9%	-27.6%	-39.9%
N-0.5	-9.4%	-17.8%	-29.5%

V. CONCLUSION

This paper presents a novel reliability-based method to quantify the capacity value of soft open points using ELCC within a Monte Carlo Simulation framework. This is a reliability-aware method which – compared to the existing literature – allows the network operator to operate their network at an adjustable reliability level subject to relevant regulations and their attitude towards risk. Optimal SOP operation is formulated as a second-order cone programming problem directly in matrix form, leading to an average optimization time of 12ms, allowing efficient integration within the probabilistic framework. A comparison between the proposed SOCP model (for SOP optimization) and the full (nonconvex) ACOPF produced the same value for the objective function with a computational time three orders of magnitude lower.

The proposed method was applied to a real distribution network operated by Taiwan Power Company considering three capacities for each SOP (0.5, 1, and 2 MVA) and three redundancy levels (N-1, N-0.75, and N-0.5). The resulting ELCC-based capacity values for five installed SOPs across the network ranged from 2.4 MVA (0.5-MVA SOPs at N-1) to 12.84 MVA (2-MVA SOPs at N-0.5). Under a relaxed redundancy level (N-0.75 and N-0.5), the capacity value for a given SOP rating increases significantly, changing by a factor of 2.36 in one case, relative to N-1. Results showed that the lower the initial network reliability level (or the higher the acceptable EENS), the higher the capacity value of the SOPs. For relaxed redundancy levels the normalized ELCC (ELCC as a proportion of SOP capacity installed) was greater than 100%.

APPENDIX A
DETERMINATION OF OBJECTIVE FUNCTION WEIGHTS

The weighted terms are included in the objective function to ensure low gaps for the relaxed second-order cone constraints, (17) and (27), without affecting the maximum proportion of substation demand that can be supplied (a). The associated weights, φ_1 and φ_2, have been determined through sensitivity analysis considering the maximum loading condition (D_t = 24 MVA) with one incoming circuit on outage (C = 16 MVA) and five 1-MVA SOPs (the test case used in Section IV-C). Three metrics were used to evaluate the accuracy of the relaxations:

$$\mathrm{Gap}_1 = \max_{ij\in\Omega_b}\left|\sqrt{L_{ij}} - \sqrt{\left(P_{ij}^2 + Q_{ij}^2\right)/u_i}\right| \tag{30}$$

which is associated with relaxed constraint (17). This gap is adjusted by φ_1. This metric is also used in [25].

$$\mathrm{Gap}_2 = \max_{i\in\Omega_{\mathrm{SOP}}}\left|P_i^{\mathrm{SOP,L}} - LC_i^{\mathrm{SOP}}\sqrt{\left(P_i^{\mathrm{SOP}}\right)^2 + \left(Q_i^{\mathrm{SOP}}\right)^2}\right| \tag{31}$$

which is associated with relaxed constraint (27). This gap is adjusted by φ_2.

Zero or relatively small gap values indicate that the relaxations are practical for the model [25]. Larger values for φ_1 and φ_2 result in smaller values for Gap_1 and Gap_2, respectively. However, if φ_1 is too large, the first weighted term substantially affects the proportion of substation demand that can be supplied (a). This reduces both a and system current. There is therefore a range of acceptable weight values which ensure both low gap values and correct value for a. This is demonstrated using the third metric, which is the absolute error of the proportion of substation demand that can be supplied (Δa) compared to the full ACOPF model, which can be defined as:

$$|\Delta a| = \left|a_{\mathrm{ACOPF}} - a_{\mathrm{SOCP}}\right| \tag{32}$$

where a_{ACOPF} and a_{SOCP} are the obtained values for a from the full ACOPF and the SOCP models, respectively. Δa should be small, indicating that the additional terms do not substantially affect the outcome of the optimization problem.

Very low values for all of the above metrics ensure a reliable solution. Table VII shows all three metrics for six combinations

of φ_1 and φ_2. Zero weights yield very high gap values, and therefore are unacceptable. A relatively high value for φ_1 (=10^{-3}) decreases Gap_1, but results in a significant error in a. The selected option (shown in bold) has a satisfactory performance across all three metrics. 0.023 A for Gap_1 compares to a mean branch current of 94 A; 1.49×10^{-6} MW for Gap_2 compares to a maximum SOP active power loss of 0.02 MW; and 4.50×10^{-6} corresponds to a = 0.8900.

TABLE VII
SELECTION OF OBJECTIVE FUNCTION WEIGHTS

φ_1	φ_2	Gap_1 (A)	Gap_2 (MW)	$\lvert\Delta a\rvert$
10^{-5}	**10^{-3}**	**0.023**	**1.49×10^{-6}**	**4.50×10^{-6}**
10^{-7}	10^{-3}	1.258	1.06×10^{-5}	1.57×10^{-7}
10^{-3}	10^{-3}	0.007	1.12×10^{-6}	0.048
10^{-5}	10^{-5}	0.045	1.92×10^{-4}	4.94×10^{-6}
10^{-5}	10^{-1}	0.065	9.58×10^{-9}	6.91×10^{-5}
0	0	392.134	0.59	3.81×10^{-7}

APPENDIX B
IMPACT OF CIRCUIT BREAKER FAILURES ON INCOMING CIRCUIT OUTAGE PROBABILITIES

The effect of the different CB failure modes on the incoming circuit availability is analyzed in this appendix. Sections B-1 and B-2 explain the contribution of different failure events to single and double circuit outage probabilities, respectively.

1) Single Circuit Outages

The failure events which lead to a single circuit outage are:

a) Active failures of overhead lines and transformers in combination with successful operation of CBs

With respect to Fig. 9, these failure events refer to active failures of components 1, 2, 4, 5 with CBs 3, 6 opening when required to do so; these events are noted as (1, 2, 4, 5)A. The corresponding unavailability ($U_{s,a}$) in h/y is:

$$U_{s,a} = \left(1 - P_{stuck}\right)\left(\lambda_{OHL} r_{OHL} + \lambda_{TX} r_{TX}\right) \tag{33}$$

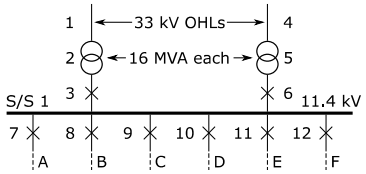

Fig. 9. Substation S/S 1 incoming circuits (with numbered components).

b) Active failures of overhead lines and transformers in combination with stuck CBs

These failure events are labelled as follows: (1, 2)A + 3S and (4, 5)A + 6S. These correspond to events in which the overhead line or the transformer of an incoming circuit actively fails and the associated CB fails to operate. This causes the operation of all other breakers, and is initially a double circuit outage; the duration of this state is equal to the substation switching time ($t_{S/S}$), which is assumed to be 30 minutes [40]. The contribution of these failure events to the probability of a double circuit outage is examined in Section B-2. Following substation switching, and until the failed component has been repaired, the outage is limited to a single circuit; this contribution is:

$$U_{s,b} = P_{stuck}\left(\lambda_{OHL}\left(r_{OHL} - t_{S/S}\right) + \lambda_{TX}\left(r_{TX} - t_{S/S}\right)\right) \tag{34}$$

c) Active failures of incoming circuit CBs

An active failure of an incoming circuit CB – (3, 6)A – causes all other CBs to operate, which initially causes a double circuit outage. The duration of this state is equal to the substation switching time ($t_{S/S}$). Subsequently, the failure is reduced to a single circuit outage until the failed CB is repaired yielding a contribution of:

$$U_{s,c} = \lambda_{CB,A}\left(r_{CB} - t_{S/S}\right) \tag{35}$$

where $\lambda_{CB,A}$ is the active failure rate of CBs.

d) Passive failures of incoming circuit CBs

A passive failure of an incoming circuit CB – (3, 6)P – does not cause the operation of any other CBs, as it is effectively an open circuit. This means that these failure events only lead to a single circuit outage until the failed CB has been repaired. The corresponding unavailability contribution is:

$$U_{s,d} = \lambda_{CB,P} r_{CB} \tag{36}$$

where $\lambda_{CB,P}$ is the passive failure rate of CBs.

Having derived all unavailability contributions for single circuit outages (a-d), we can now calculate the circuit availability (A_C) as follows:

$$A_C = \left(8760 - \left(U_{s,a} + U_{s,b} + U_{s,c} + U_{s,d}\right)\right)/8760 \tag{37}$$

The probability of a single circuit outage (p_{1C}) is therefore:

$$p_{1C} = 2\left(1 - A_C\right) - \left(1 - A_C\right)^2 \tag{38}$$

2) Double Circuit Outages

The failure events which result in a double circuit outage are:

a) Active failures of overhead lines and transformers in combination with stuck CBs

As discussed in Section B-1b, these failure events – (1, 2)A + 3S and (4, 5)A + 6S – lead to a double circuit outage for a duration equal to the substation switching time. The corresponding contribution to unavailability is:

$$U_{d,a} = 2P_{stuck}\left(\lambda_{OHL} + \lambda_{TX}\right)t_{S/S} \tag{39}$$

b) Active failures of incoming circuit CBs

Similarly, active failures of incoming circuit CBs – (3, 6)A – cause a double circuit outage until switching at the substation has been completed. The unavailability contribution is:

$$U_{d,b} = 2\lambda_{CB,A} t_{S/S} \tag{40}$$

c) Active failures of feeder CBs

Active failures of feeder CBs – (7-12)A – result in a double circuit outage during substation switching time. Following that, only the feeder is affected, and both incoming circuits are available. The contribution is:

$$U_{d,c} = N_{FCBs}\lambda_{CB,A} t_{S/S} \tag{41}$$

where N_{FCBs} is the number of feeder CBs.

d) Two overlapping single circuit outages

The final contribution is that of the overlapping single circuit outages. The corresponding probability is $(1\text{-}A_C)^2$, which yields the following unavailability (in h/y):

$$U_{d,d} = 8760\left(1 - A_C\right)^2 \tag{42}$$

We have now computed all double circuit outage contributions (a-d). The associated probability (p_{0C}) is:

$$p_{0C} = \left(U_{d,a} + U_{d,b} + U_{d,c} + U_{d,d}\right) / 8760 \quad (43)$$

The probability both incoming circuits are intact (p_{2C}) is:

$$p_{2C} = 1 - p_{1C} - p_{0C} \quad (44)$$

Table VIII summarizes the unavailability contributions of each failure event to single and double circuit outages. Table IX provides reliability data for 11kV CBs. Failure rates and repair time are taken from [30], the stuck-breaker probability is obtained from [35] (confidential), and substation switching time is acquired from [40].

TABLE VIII
SUMMARY OF UNAVAILABILITY CONTRIBUTIONS OF THE DIFFERENT FAILURE EVENTS TO SINGLE AND DOUBLE CIRCUIT OUTAGES

Failure Events	Unavailability Contribution	
	Single Circ. Out.	Double Circ. Out.
(1, 2, 4, 5)A	$U_{s,a}$	–
(1, 2)A + 3S, (4, 5)A + 6S	$U_{s,b}$	$U_{d,a}$
(3, 6)A	$U_{s,c}$	$U_{d,b}$
(3, 6)P	$U_{s,d}$	–
(7-12)A	–	$U_{d,c}$
Overlapping single outages	–	$U_{d,d}$

TABLE IX
11 KV CIRCUIT BREAKER RELIABILITY DATA

Parameter	Value
Active Failure Rate ($\lambda_{CB,A}$)	0.004 f/y
Passive Failure Rate ($\lambda_{CB,P}$)	0.002 f/y
Repair Time (r_{CB})	4 h
Stuck-Breaker Probability (P_{stuck})	Confidential
Substation Switching Time ($t_{S/S}$)	0.5 h

ACKNOWLEDGMENTS

The first author would like to thank Mrs Antigone Mondelou for her valuable advice and support. Also, the authors would like to thank three anonymous reviewers for their comments which have greatly improved the manuscript.

This work was supported by Northern Powergrid, UK as part of the Pragmatic Security Assessment NIA Project (NIA_NPG_029), and as part of the Enhanced Understanding of Network Losses Project.

This work was also supported by the Engineering and Physical Sciences Research Council (EPSRC) grant number EP/T021969/1, and National Science Foundation of China (NSFC) grant number 520616336103, under NSFC-EPSRC Collaborative Research Initiative in Sustainable Power Supply, as part of the Multi-energy Control of Cyber-Physical Urban Energy Systems (MC2) Project.

Data supporting this publication are available at: https://doi.org/10.25405/data.ncl.14357345.

REFERENCES

[1] W. Cao, J. Wu, N. Jenkins, C. Wang, and T. Green, "Benefits analysis of Soft Open Points for electrical distribution network operation," *Appl. Energy*, vol. 165, pp. 36-47, 2016.

[2] E. Romero-Ramos *et al*., "Assessing the loadability of active distribution networks in the presence of DC controllable links," *IET Gener. Transm. Distrib.*, vol. 5, no. 11, pp. 1105-1113, 2011.

[3] G. Strbac et al., "Benefits of Advanced Smart Metering for Demand Response based Control of Distribution Networks, Report for the Energy Networks Association," 2010.

[4] L. L. Garver, "Effective Load Carrying Capability of Generating Units," *IEEE Trans. Power App. Syst.*, vol. PAS-85, no. 8, pp. 910-919, 1966.

[5] M. Amelin, "Comparison of Capacity Credit Calculation Methods for Conventional Power Plants and Wind Power," *IEEE Trans. Power Syst.*, vol. 24, no. 2, pp. 685-691, 2009.

[6] Y. Zhou, P. Mancarella, and J. Mutale, "Framework for capacity credit assessment of electrical energy storage and demand response," *IET Gener. Transm. Distrib.*, vol. 10, no. 9, pp. 2267-2276, 2016.

[7] I. Sarantakos, D. M. Greenwood, N.-M. Zografou-Barredo, V. Vahidinasab, and P. C. Taylor, "A probabilistic method to quantify the capacity value of load transfer," *Int. J. Elect. Power Energy Syst.*, 2020.

[8] C. J. Dent, A. Hernandez-Ortiz, S. R. Blake, D. Miller, and D. Roberts, "Defining and Evaluating the Capacity Value of Distributed Generation," *IEEE Trans. Power Syst.*, vol. 30, no. 5, pp. 2329-2337, 2015.

[9] M. Ding and Z. Xu, "Empirical Model for Capacity Credit Evaluation of Utility-Scale PV Plant," *IEEE Trans. Sustain. Energy*, vol. 8, no. 1, pp. 94-103, 2017.

[10] Y. G. Hegazy, M. M. A. Salama, and A. Y. Chikhani, "Adequacy assessment of distributed generation systems using Monte Carlo Simulation," *IEEE Trans. Power Syst.*, vol. 18, no. 1, pp. 48-52, 2003.

[11] I. Konstantelos and G. Strbac, "Capacity value of energy storage in distribution networks," *Journal of Energy Storage*, 2018.

[12] Imperial College London, "Review of Distribution Network Security Standards," 2015.

[13] D. M. Greenwood, N. S. Wade, P. C. Taylor, P. Papadopoulos, and N. Heyward, "A Probabilistic Method Combining Electrical Energy Storage and Real-Time Thermal Ratings to Defer Network Reinforcement," *IEEE Trans. Sustain. Energy*, vol. 8, no. 1, pp. 374-384, 2017.

[14] R. Billinton and R. N. Allan, *Reliability Evaluation of Power Systems*, 2nd ed. New York: Plenum, 1996.

[15] S. Giannelos, I. Konstantelos, and G. Strbac, "Option value of Soft Open Points in distribution networks," in *IEEE Eindhoven PowerTech*, 2015.

[16] I. Konstantelos, S. Giannelos, and G. Strbac, "Strategic Valuation of Smart Grid Technology Options in Distribution Networks," *IEEE Trans. Power Syst.*, vol. 32, no. 2, pp. 1293-1303, 2017.

[17] J. Wang, N. Zhou, C. Y. Chung, and Q. Wang, "Coordinated Planning of Converter-Based DG Units and Soft Open Points Incorporating Active Management in Unbalanced Distribution Networks," *IEEE Trans. Sustain. Energy*, pp. 1-1, 2019.

[18] R. Billinton and W. Li, *Reliability Assessment of Electric Power Systems Using Monte Carlo Methods*. New York: Plenum, 1994.

[19] Energy Networks Association, "Engineering Recommendation P27: Current rating guide for high voltage overhead lines operating in the UK distribution system," 1986.

[20] M. Farivar, C. R. Clarke, S. H. Low, and K. M. Chandy, "Inverter VAR control for distribution systems with renewables," in *2011 IEEE International Conference on Smart Grid Communications (SmartGridComm)*, 2011.

[21] M. Farivar and S. H. Low, "Branch Flow Model: Relaxations and Convexification—Part I," *IEEE Trans. Power Syst.*, vol. 28, no. 3, pp. 2554-2564, 2013.

[22] H. Ji, C. Wang, P. Li, F. Ding, and J. Wu, "Robust Operation of Soft Open Points in Active Distribution Networks With High Penetration of Photovoltaic Integration," *IEEE Trans. Sustain. Energy*, vol. 10, no. 1, pp. 280-289, 2019.

[23] M. E. Baran and F. F. Wu, "Network reconfiguration in distribution systems for loss reduction and load balancing," *IEEE Trans. Power Del.*, vol. 4, no. 2, pp. 1401-1407, Apr. 1989.

[24] M. E. Baran and F. F. Wu, "Optimal capacitor placement on radial distribution systems," *IEEE Trans. Power Del.*, 1989.

[25] K. Chen, W. Wu, B. Zhang, S. Djokic, and G. P. Harrison, "A Method to Evaluate Total Supply Capability of Distribution Systems Considering Network Reconfiguration and Daily Load Curves," *IEEE Trans. Power Syst.*, vol. 31, no. 3, pp. 2096-2104, 2016.

[26] C.-T. Su and C.-S. Lee, "Network reconfiguration of distribution systems using improved mixed-integer hybrid differential evolution," *IEEE Trans. Power Del.*, vol. 18, no. 3, pp. 1022-1027, 2003.

[27] I. Sarantakos, D. M. Greenwood, J. Yi, S. R. Blake, and P. C. Taylor, "A method to include component condition and substation reliability into distribution system reconfiguration," *Int. J. Elect. Power Energy Syst.*, vol. 109, pp. 122-138, 2019.

[28] *Statutory Instruments, The Electricity Safety, Quality and Continuity Regulations 2002, No. 2665*, 2002.

[29] National Grid, "Current Ratings for Overhead Lines," 2001.

[30] R. N. Allan, R. Billinton, I. Sjarief, L. Goel, and K. S. So, "A reliability test system for educational purposes – Basic distribution system data and results," *IEEE Trans. Power Syst.*, vol. 6, no. 2, pp. 813-820, 1991.

[31] Gurobi Optimization LLC. "Gurobi Optimizer Reference Manual." http://www.gurobi.com.
[32] D. T. C. Wang, L. F. Ochoa, and G. P. Harrison, "DG Impact on Investment Deferral: Network Planning and Security of Supply," *IEEE Trans. Power Syst.*, vol. 25, no. 2, pp. 1134-1141, 2010.
[33] D. M. Greenwood and P. C. Taylor, "Unlocking the benefits of real-time thermal ratings through probabilistic power network planning," *IET Gener. Transm. Distrib.*, vol. 8, no. 12, pp. 2055-2064, 2014.
[34] J. Lofberg, "YALMIP : a toolbox for modeling and optimization in MATLAB," in *IEEE International Conference on Robotics and Automation*, 2004.
[35] CE Electric UK (Commercial in Confidence), "Failure on Demand of Primary Feeder Circuit Breakers," 2009.
[36] L. Gan and S. H. Low, "Convex relaxations and linear approximation for optimal power flow in multiphase radial networks," in *Power Systems Computation Conference (PSCC)*, 2014.
[37] P. Li *et al.*, "Optimal Operation of Soft Open Points in Active Distribution Networks Under Three-Phase Unbalanced Conditions," *IEEE Trans. Smart Grid*, vol. 10, no. 1, pp. 380-391, 2019.
[38] "Renewables.ninja." https://www.renewables.ninja/.
[39] MOSEK ApS. "The MOSEK Optimization Tools Version 9.1.6." http://www.mosek.com/.
[40] R. E. Brown and T. M. Taylor, "Modeling the impact of substations on distribution reliability," *IEEE Trans. Power Syst.*, 1999.

Ilias Sarantakos received the Dipl. Ing. degree from the School of Electrical and Computer Engineering, National Technical University of Athens, Greece, in 2013, and the Ph.D. degree from the School of Engineering, Newcastle University, UK, in 2019.

Since 2018 he has been a Postdoctoral Researcher with the Electrical Power Research Group, Newcastle University. His research interests include distribution network operation and planning, optimization, reliability, and security of supply.

Natalia-Maria Zografou-Barredo received the Diploma Ing. degree from the Department of Electrical and Computer Engineering, School of Engineering, University of Patras, Greece, in 2016. She is currently pursuing the Ph.D. degree in electrical and electronic engineering with the School of Engineering, Newcastle University, U.K.

Her current research interests include distribution network operation, active network management, microgrid operation, and mathematical optimization.

She is the recipient of the 2016 IEEE Greece Power and Energy Society POWERED Award (16th Workshop on Power Engineering Dissertations).

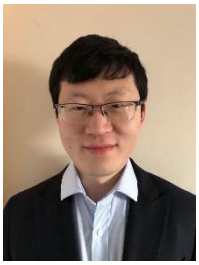

Da Huo received the B.Eng. degrees in Electrical and Electronic Engineering from the University of Bath, U.K., and in Electrical Power Engineering from North China Electric Power University, Baoding, China, both in 2014. He received the Ph.D. degree from the University of Bath, U.K., in 2018. He is currently a research associate with the School of Engineering, Newcastle University. His main research interests are the multi-vector systems and energy trading.

David Greenwood (M'14) received the M.Eng. degree in new and renewable energy from Durham University, Durham, U.K., in 2010 and the Ph.D. degree, for work on real-rime thermal ratings, from Newcastle University, Newcastle upon Tyne, U.K., in 2014. He is a Newcastle University Academic Track Fellow focussing on whole systems approaches to energy.